HIRDLS/ISAMS Vertical Resolution Study

JJB, AJLM, 23 February 1990 (version 2)

1. Aims of the study

The aim of the study is to quantitatively determine the optimum vertical instrument field of view (IFOV) and the sampling strategy. It complements retrieval simulation studies, in providing an understanding of factors that limit the resolution and in being very much less demanding of computer resources. The study was performed primarily for HIRDLS but is of great relevance for ISAMS which has an IFOV of about 2.36 km and a view direction step size of about half of this. In addition the results from section 3 have a broader application to deconvolution problems, such as the improvement of HIRDLS along-track resolution.

2. Backus and Gilbert analysis

The study was conducted using the concepts developed by Backus and Gilbert (1967, 1970) and applied to atmospheric sounding by Conrath (1972). The technique generates linear combinations of input weighting functions that minimise various combinations of noise for that combination and its 'spread'.

Suppose that radiances for each of m weighting functions $W_i(z')$ are measured by the instrument where i takes values if 1 to m. z' is the height coordinate. We linearly combine them with coefficients a_i to give a combination weighting function $A(z, z')$ used to sound some desired height z such that:

$$A(z, z') = \sum_{i=1}^{m} a_i W_i(z).$$

'Spread' S is roughly equivalent to width or resolution, and is defined as

$$S(z) = 12 \int_0^\infty (z - z')^2 A^2(z, z') dz'.$$

This definition has the advantage that the problem can be solved analytically. The factor of 12 causes the spread of a boxcar function centred on the desired level to have a spread equal to its width. The variance E_A corresponding to A is given by

$$E_A = \sum_{i=1}^{m} a_i \sum_{j=1}^{m} E_{ij} a_j$$

where E_{ij} is the error covariance between measurements i and j. For this application off-diagonal elements of matrix **E** are taken to be zero, and the diagonal elements are taken all to be equal to the instrument noise variance.

For a given height z various sets of coefficients a_i are obtained algebraically be minimising the sum of $qS(z) + (q - 1)rE(z)$ where q is chosen by the user and has a value between 0 and 1, and r is a dimensioned constant also chosen by the user to the scale the problem in a convenient way. Setting q to 0 will lead to a combination which minimises the error of the combination function irrespective of its spread (in this case the combination will be an average of all of the input functions with $a_i = m^{-1}$). Setting q to 1 will lead to the combination with lowest spread irrespective of noise. Intermediate values of q lead to compromise solutions which are normally preferable. Results are given in the form of a tradeoff curve (delineated usinmg a large set of different values of q) showing how noise varies with spread. In principle the user can use the curve to help select which tradeoff

to use, but in this case tradeoff curves will be generated for different values of IFOV and then intercompared.

3. Measurement of Limb Radiance profiles

A set of idealised field of view functions was first studied, as shown in figures 1a-d. These are Gaussians of full width at half height of 2 km. Set (a) has 9 functions at 2 km intervals between centres. Sets (b), (c) and (d) use 17, 25 and 33 functions to span the same height range, hence are spaced at intervals of 1, 0.667 and 0.5 km respectively. Figure 2 gives three examples of combinations centred half way up the family of 25 functions. One example is the narrowest obtainable, another is that of lowest noise (it is the average of all of the input functions), and the third is some compromise.

Figures 3a and 3b give the tradeoff curves for (a) a level centred on the centre function, and (b) half way between the centre function and the next above. The various points are for different trade-offs between width and noise for each of the 4 sets of input functions. (The origin of the points cannot be distinguished since the colour on the original has been lost in reproduction). The points all fall on the same curve with the exception of those for 9 functions which deviate markedly below the curve for case (a) and above for case (b). This is intuitively to be expected since we might expect the best resolution to be obtained for the case of adjacent, non-overlapping functions, when a function is centred on a desired level, and the worst when the required level is midway between function centres. In this case the resolution varies with height but has an average value that approximately follows the tradeoff curve for closer function spacing. Although a non-oversampled set of weighting functions appears to give better value if measurements are only required at weighting function centres, oversampling does lead to a lower limiting spread (it cannot lead to a worse spread because the set contains all of the weighting functions present in the non-oversampled case but with higher noises).

It can be seen that the limiting minimum spread is approximately 0.9 km, and that a spread of 1 km (i.e. half of the full width at half height of the Gaussian weighting functions) is obtained with a noise amplification of approximately 10× compared with that for 2 km spread.

When making these composite tradeoff curves, the noise for each measurement has been assumed to be proportional to $m^{1/2}$ where m is the number of functions; this is consistent with the instrument using a fixed amount of time to obtain a complete set. The vertical scale (noise) should be considered to be arbitrary in this case.

Tradeoff curves for narrower or wider input functions can be generated by shifting the curves (plotted on log-log axes). Consider using detectors 1km wide. If the scan range is halved we have precisely the same problem with all of the distance scales halved. However the noise in radiance units for a given integration time will be $2^{1/2}$ higher because the detectors are smaller. In addition with the scan range halved the instrument can only spend half of its time scanning this part of the atmosphere. The net result is that the tradeoff curve is shifted upwards and to the left by and amount corresponding to a factor of 2 in each direction.

4. Measurement of profiles of geophysical quantities

The above case corresponds to measurements and analysis of profiles of radiance as observed from space. We can measure them to any desired resolution by providing sufficient optical resolution. In order to retrieve temperature or concentration or mixing ratio of a species as a function of radial distance from the earth's centre we must take into account

vertical averaging caused by the viewing geometry which imposes a practical limit on the ultimate vertical resolution.

4.a. Weighting functions

Figure 4a-c give functions that have been used to determine the tradeoff between resolution and noise for IFOVs of 1, 1.5 and 2 km respectively; the functions used for 1.25 km IFOV are not shown. In each case a detector of this projected height in the atmosphere is assumed together with a 16 cm entrance aperture with diffraction appropriate to 15 micron wavelength radiation, and additional aberration with a spot diameter at the focal plane of 30 microns assuming f1.5 optics. This gives rise to the rounded-off boxcar function in each figure (the curves labelled optical). That curve has been further convolved with the sharply peaked atmospheric smoothing function which gives the number of molecules per unit height along a tangent path for a gas whose concentration has a scale height of 7 km. This curve is appropriate for sounding a gas of uniform mixing ratio when the passband includes the whole of spectral lines (centres plus wings) and when the centres are optically thin. (For optically thick centres and scale height of 14km would be more appropriate implying broader atmospheric smoothing functions.)

The convolved functions have been replicated as shown in figures 5a-c, 6a-b, 7a-c and 8a-c for IFOVs of 1, 1.25, 1.5 and 2 km respectively. In each case curves a, b and c have peaks spaced at the IFOV, 0.5×IFOV and 0.25×IFOV respectively giving no oversampling (abutting fields of view except for any diffraction and aberration effects) for cases (a), and various degrees of oversampling for (b) and (c). The areas under the curves are unity for the centre function which has the centre of the IFOV located at 10 km. Other functions have an area of $\exp(-(z-10)/7)$ where z is the height (km) of the centre of the IFOV.

Three methods were considered in order to obtain equivalent IFOV scan range for measurements with different resolutions so that valid comparison would be possible:

a) equal scan range of the IFOV centres;
b) equal distance from the bottom of the lowest detector edge to the top of the highest detector edge;
c) a more sophisticated version of (b) to allow for the effect of atmospheric and optical broadening, e.g. equal distance from Δ_1 below the bottom IFOV centre to Δ_2 above the top IFOV centre where Δ_1 and Δ_2 are the distances from the centre of the lower and upper half power points of the convolved functions as given in figure 4.

Method (a) was used, with a scan range of 16 km (IFOV centres at 2-18 km) except for the 1.5 km IFOV where 15 km was used because the computational grid did not permit a range of 16 km. Ideally the noise for the 1.5 km cases should be increased by $\approx (16/15)^{1/2}$ to allow for the reduced scan range, but this was not done. Differences between methods a, b and c above are of similar magnitude and are probably sufficiently small as to be ignored.

Having arranged for the different cases to have equivalent scan ranges, the noise of each measurement was set to $(m/w)^{1/2}$, where m is the number of functions and w is the IFOV width measured in km.

4.b. Intercomparison of test cases for 10 km

Figure 9a gives the full tradeoff curves for each case on log-log scales and figure 9b gives a subset of the domain on linear scales. In figure 9a it can be verified that for large spreads the wider IFOV gives rise to lower noise. The oversampled curves for 2 km IFOV cross the remainder at about 2 km resolution, although the non-oversampled 2 km

IFOV cases continues to much smaller spreads for reasons discussed in the next section. The curves for 1, 1.25 and 1.5 km IFOV cross each other at a spread of about 1.3 km, with the 1 km IFOV providing some advantage over that for 1.25 km, but only for noise amplification more than twice that obtained for 2 km resolution for the 1.25 and 1.5 km IFOV curves.

For each IFOV width the required combination has been specified for the peak of the function which has an IFOV centred on 10 km. Such a choice is intuitively assumed to give the best vertical resolution. These heights are 10.375 km, 10.5 km, 10.625 km and 10.8125 km for 1, 1.25, 1.5 and 2 km IFOVS respectively. This has the effect of favouring the 1 km cases with a noise lower by a factor of $\exp(0.4375/7) = 1.06$ compared with the 2 km cases since the combined functions are obtained for a level of greater emission. It would be valid to multiply by this factor to correct the curves for this effect for low spreads (but consideration of the limiting minimum noise case shows that such correction is not universally valid); however this has not been done. Again the factors involved are probably too small to matter.

4.c. Variation of resolution and noise for the 2 km non-oversampled case

Figures 10a and 10b give log-log and linear-linear tradeoff curves for 2 km IFOVs provided at 2 km centres. The results of section 3 lead us to expect that the resolution will vary cyclically with height, being best near the weighting function peaks, and worst between those peaks. Because of the difficulty referred to in section 4b of correcting noise values of tradeoff curves to a common height, no correction was attempted, and instead tradeoff curves were computed for points over 3 cycles of expected variation, i.e. over 6 km, so that the vertical progression could be inspected. The heights selected were 8.8125, 10.8125 and 12.8125 km which corresponded to the weighting function peaks, and levels relative to them of ± 0.5 km and ± 1 km. Figure 10a shows that the noise levels increase with increasing value of required height, and that those for 8.3125, 10.3125 and 12.3125 km give consistently the best limiting resolution (about 1.9 km) and those 1 km out of phase give the worst resolution. Resolution for 8.8125, 10.8125 and 12.8125 km was close to the best. No doubt more extreme values of spread occur at other points in the cycle, although there is little value to finding them.

5. References

Backus, G.E. and J.F.Gilbert, 1967, Numerical Application of a Formalism for Geophysical Inverse Problems. Geophys. J. Roy. Astron. Soc., 13, 247-276.

Backus, G.E. and J.F.Gilbert, 1970, Uniqueness in the Inversion of Inaccurate Gross Earth Data. Phil. Trans. Roy. Soc. Lond. A266, 123-192.

Conrath, B.J., 1972, Vertical Resolution of Temperature Profiles Obtained from Remote Radiation Measurements. J. Atmos. Sci, 29, 1262-1271.

Figures

Figure 1. Input weighting functions used for the study described in section 3. The functions are Gaussians of 2 km full width at half height, spaced at intervals of:
(a) 2 km, (b) 1 km, (c) 0.667 km, (d) 0.5 km.

Figure 2. Averaging kernels obtained from the weighting functions given in figure 1c (0.667 km spacing) for minimum noise, minimum spread and an intermediate tradeoff.

Figure 3. Tradeoff curves for the weighting functions given in figure 1:
a) for the centre of the centre weighting function of each set (13.3 km height);
b) half way between the centre peak and the peak above.

Figure 4. Weighting functions used as the basis for the study described in section 4. In each figure is given the optical response function (as described in the text), an atmospheric smoothing function corresponding to a vertical scale height of absorption per unit volume of 7 km (this function has infinite value at the tangent height), and the convolution of these two functions. The figures are for IFOVs of:
(a) 1 km, (b) 1.5 km, (c) 2 km.

Figure 5. Input weighting functions for 1 km IFOV:
(a) 1 km function spacing;
(b) 0.5 km function spacing;
(c) 0.25 km function spacing.

Figure 6. Input weighting functions for 1.25 km IFOV:
(a) 1.25 km function spacing;
(b) 0.75 km function spacing.

Figure 7. Input weighting functions for 1.5 km IFOV:
(a) 1.5 km function spacing;
(b) 0.75 km function spacing;
(c) 0.375 km function spacing.

Figure 8. Input weighting functions for 2 km IFOV:
(a) 2 km function spacing;
(b) 1 km function spacing;
(c) 0.5 km function spacing.

Figure 9. Tradeoff curves based on the weighting functions given in figures 5-8 for heights of the peak of the central weighting function (i.e. that with a tangent height of 10 km). Note that the originals were in colour, hence the curves cannot easily be distinguished. (a) and (b) give the same data but (a) is on log-log scales and (b) is a subset on linear scales.

Figure 10. Tradeoff curves based on the weighting functions given in figure 8a for a 2 km IFOV at 2 km centres. Combinations are obtained for heights from 7.8125 km to 13.8125 km in steps of 0.5 km (i.e. over 3 IFOV widths). Note that the originals were in colour, hence the curves cannot easily be distinguished. (a) and (b) give the same data but (a) is on log-log scales and (b) is a subset on linear scales.

Figure 1a

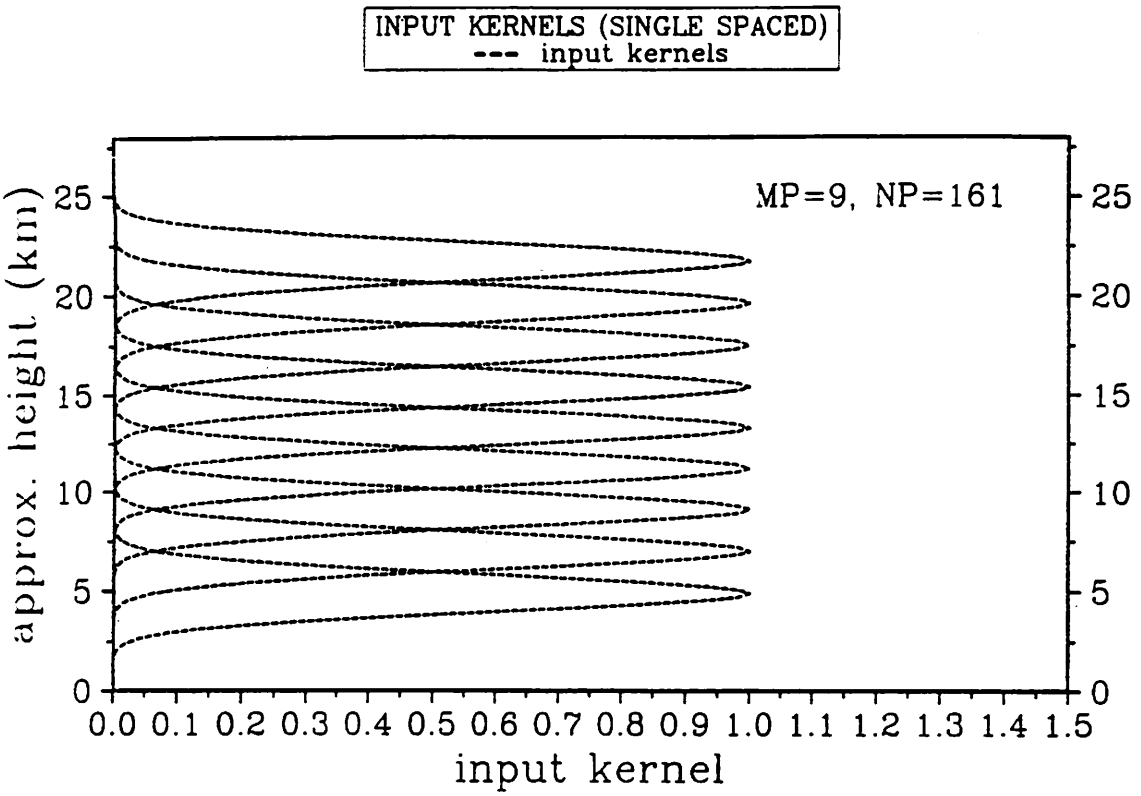

Figure 1b

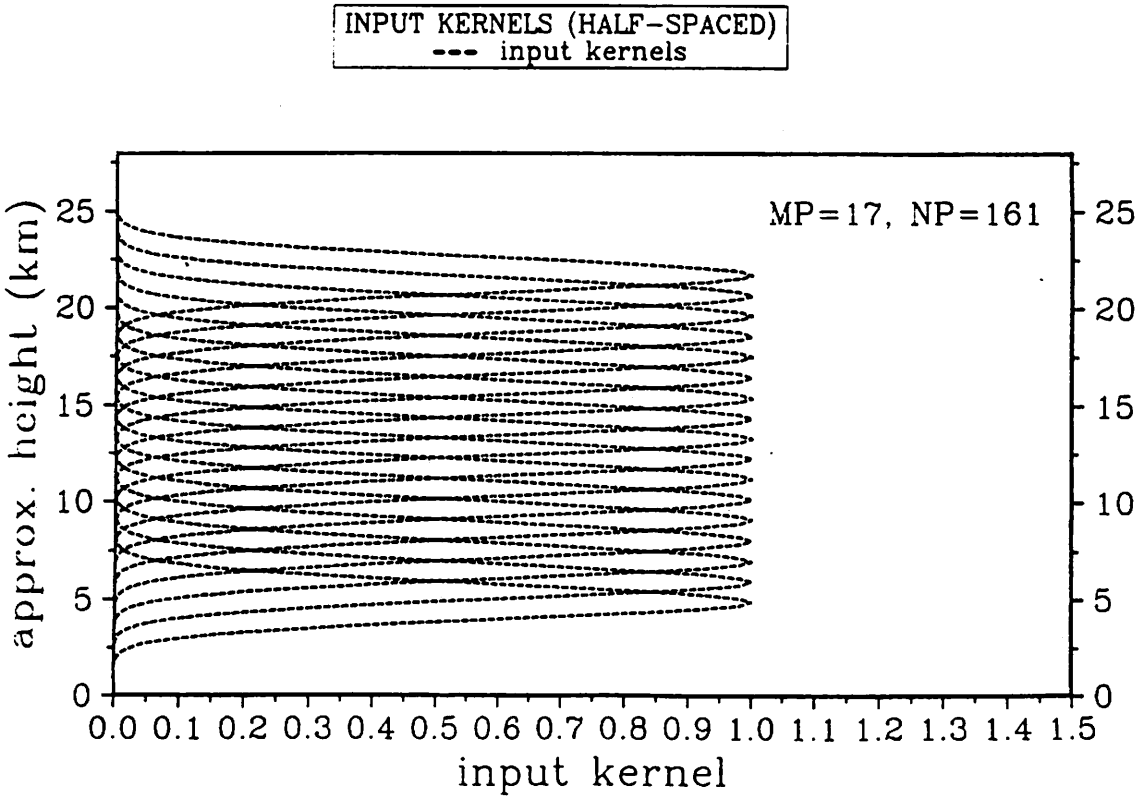

Figure 1c

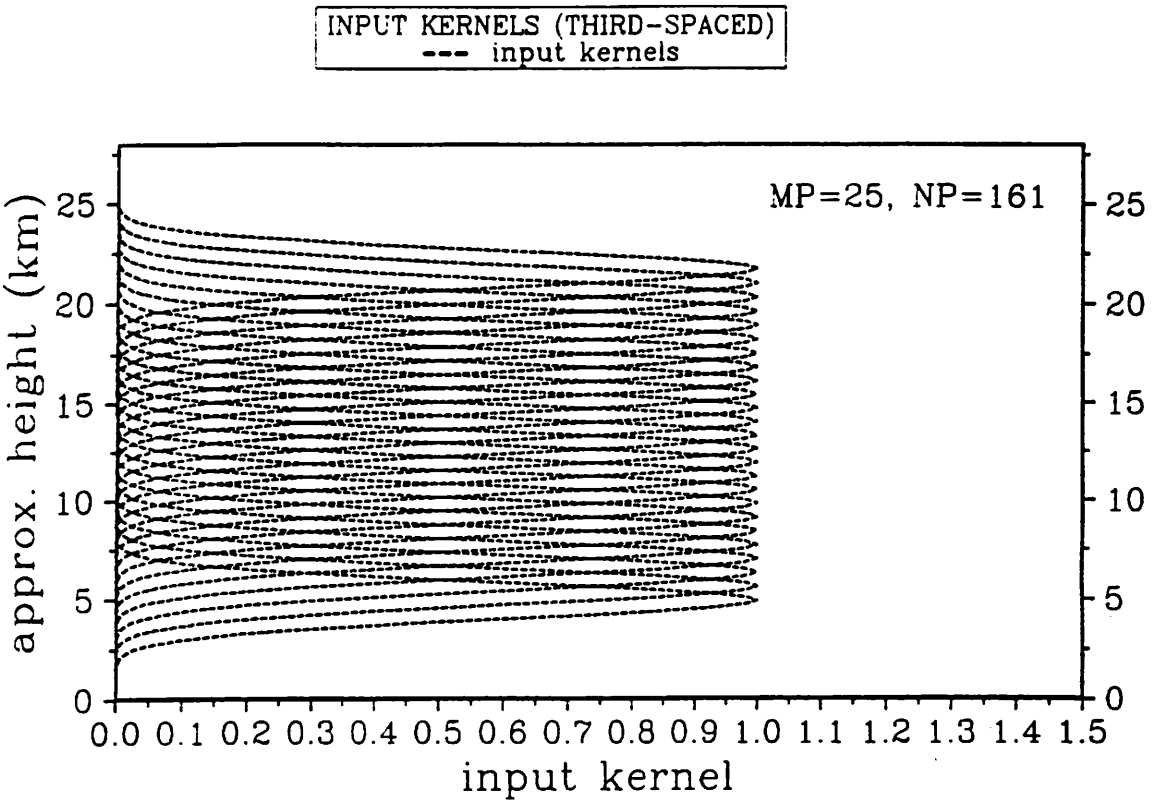

Figure 1d

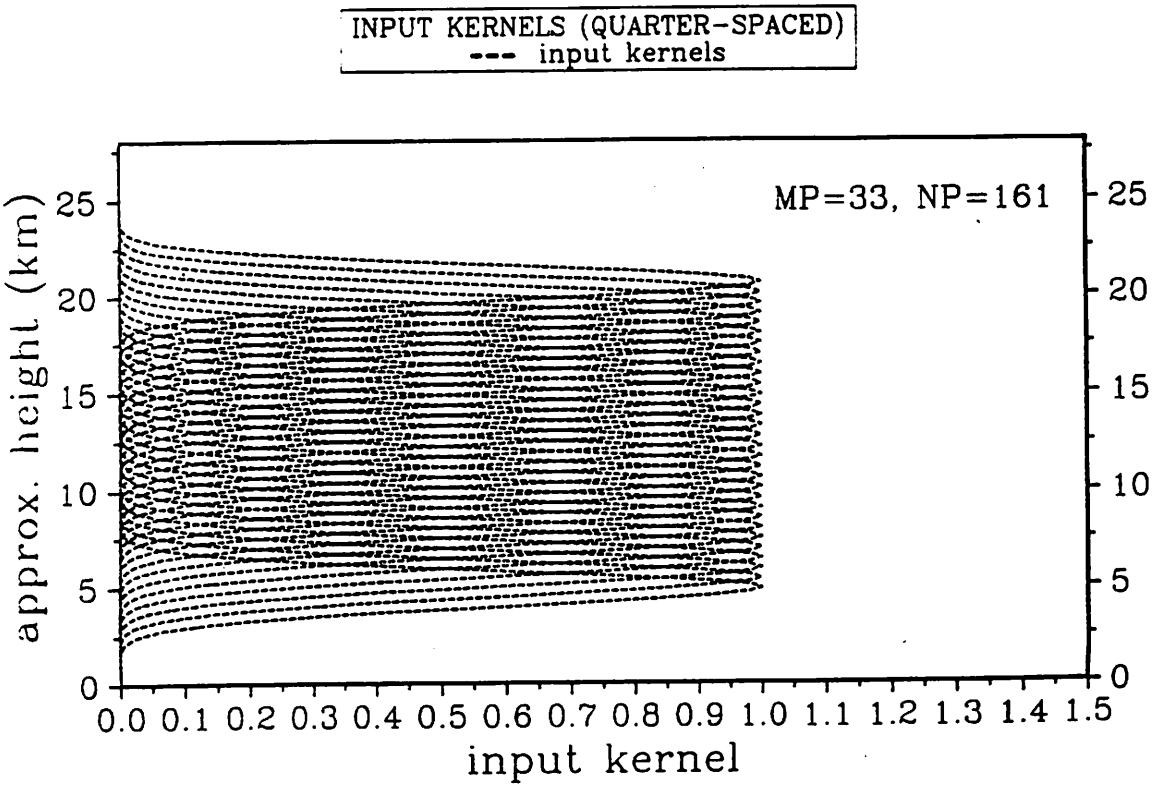

3 kernels not plotted: array size too large

Figure 2

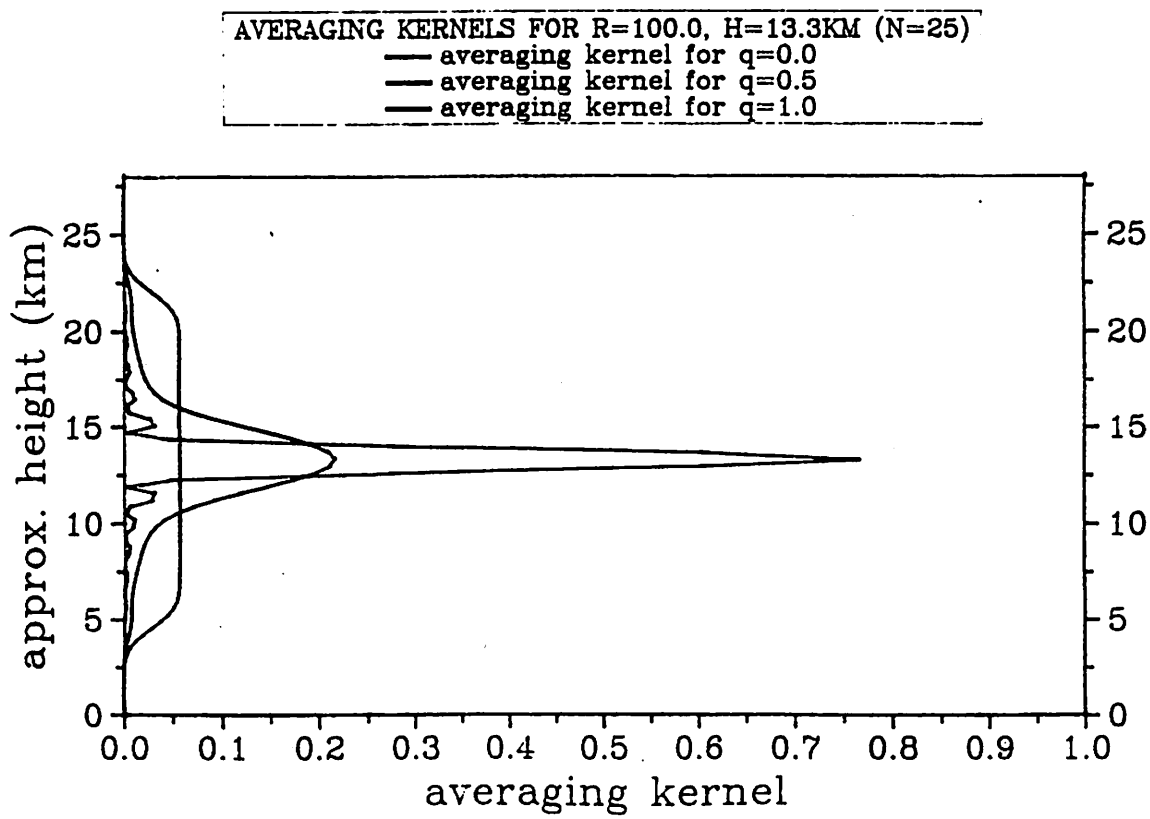
AVERAGING KERNELS FOR R=100.0, H=13.3KM (N=25)
averaging kernel for q=0.0
averaging kernel for q=0.5
averaging kernel for q=1.0
approx. height (km)
0
5
10
15
20
25
0.0
0.1
0.2
0.3
0.4
0.5
0.6
0.7
0.8
0.9
1.0
averaging kernel

Figure 3a

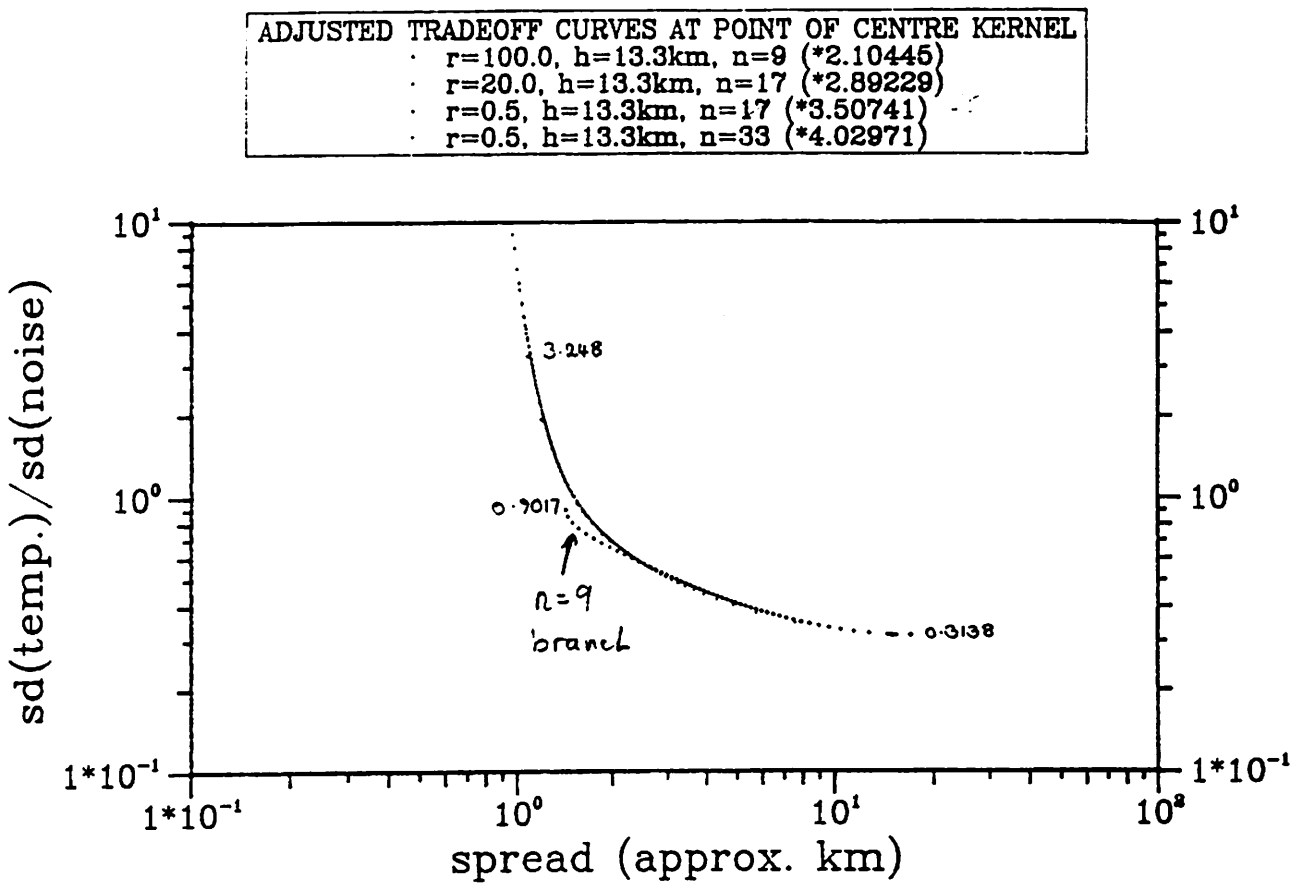

Figure 3b

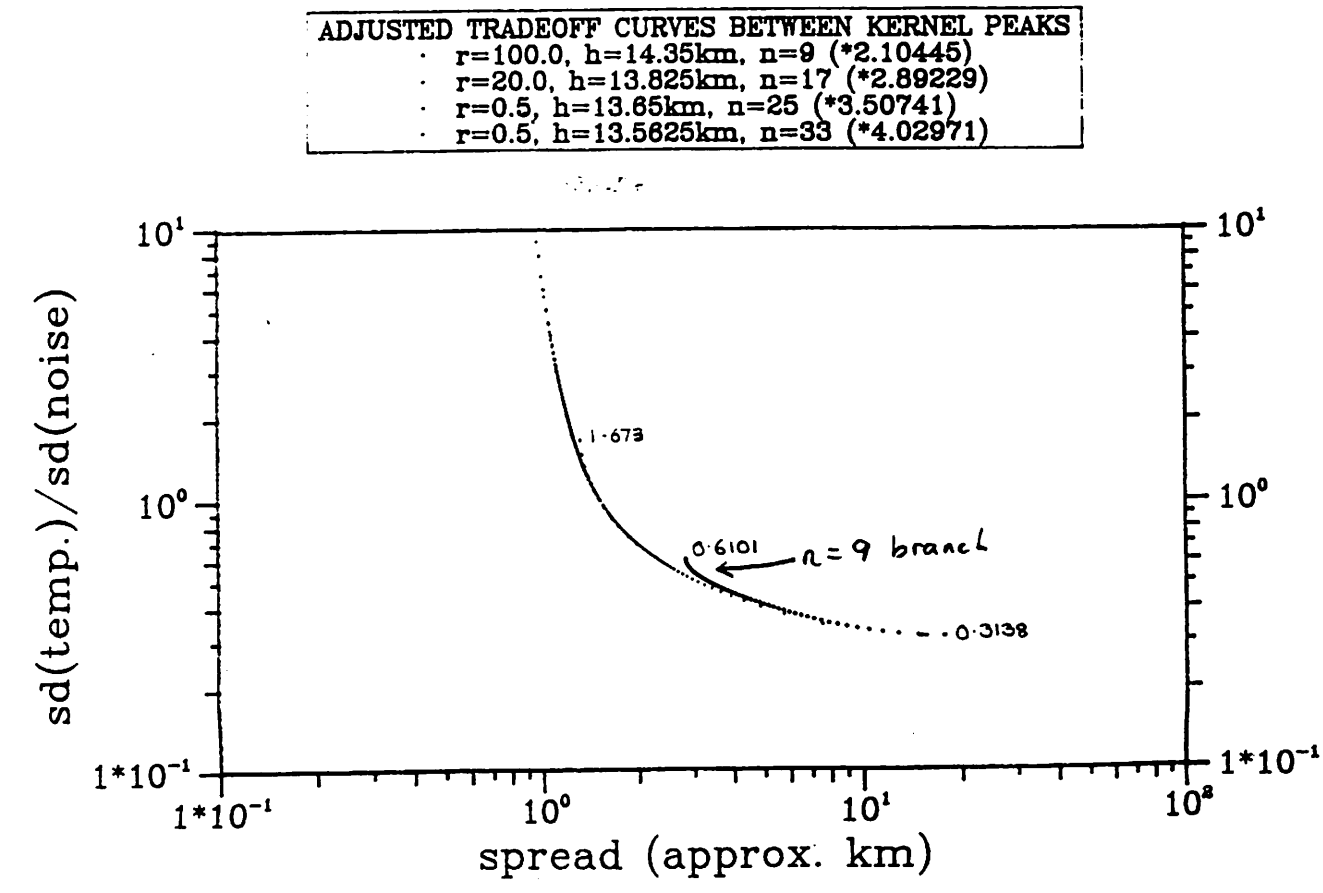

Figure 4a (1km FOV)

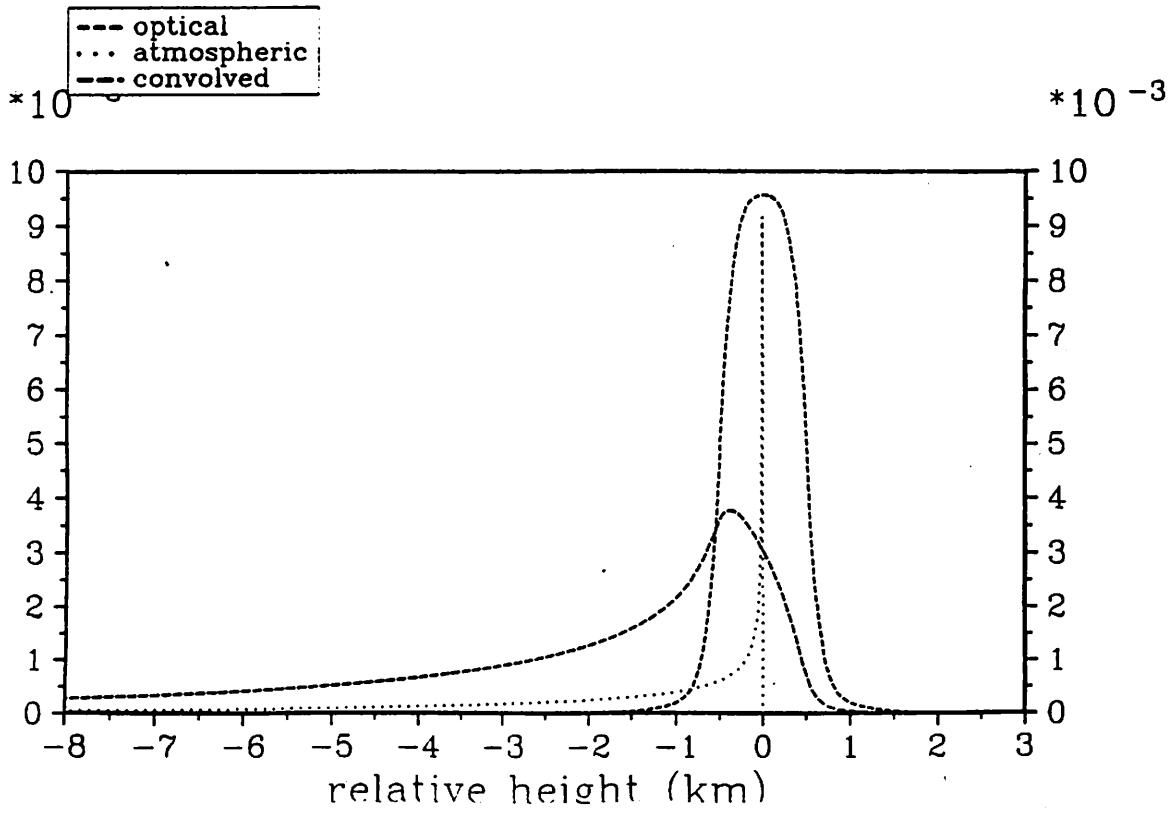

Figure 4b (1.5 km FOV)

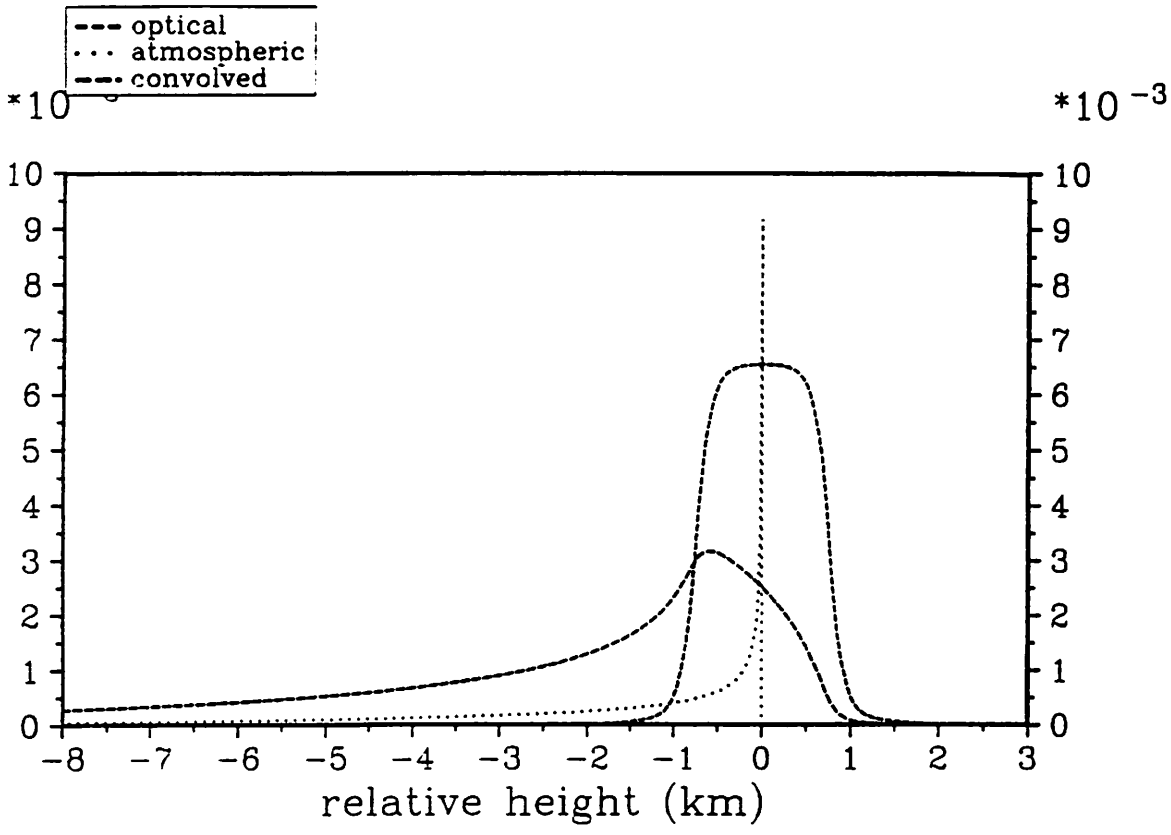

Figure 4c (2 km FOV)

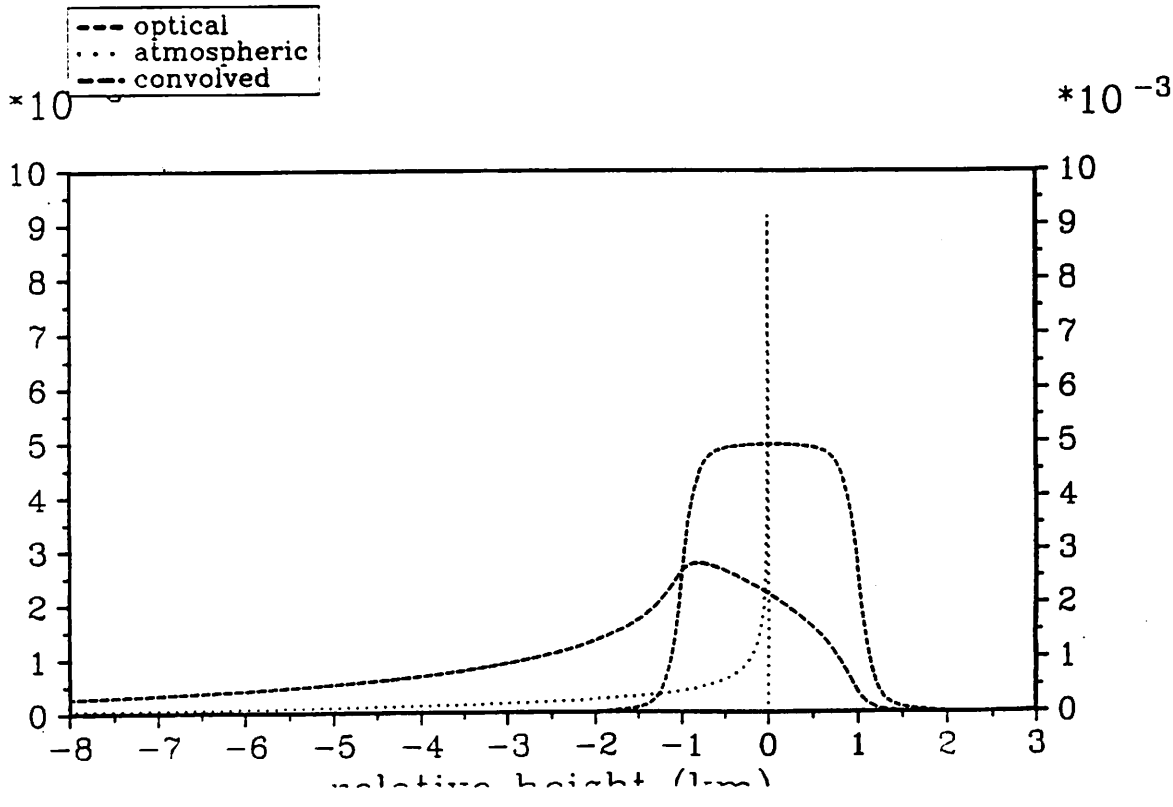

Figure 5a

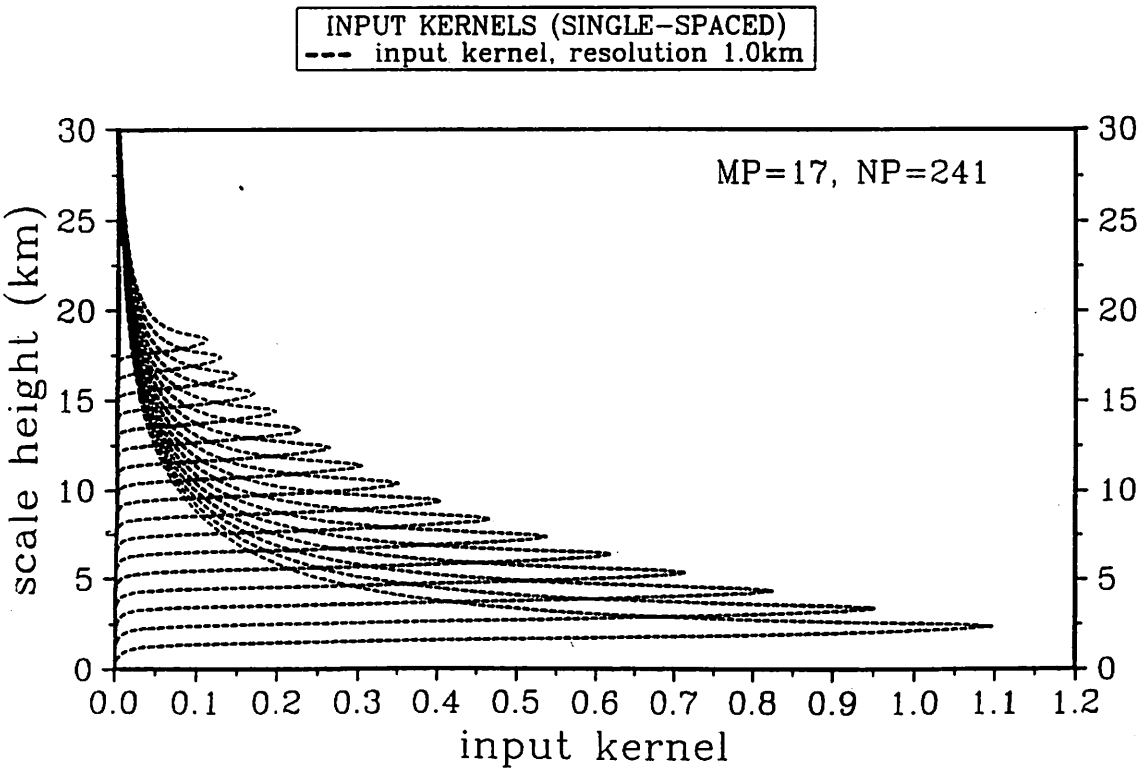
INPUT KERNELS (SINGLE-SPACED)
--- input kernel, resolution 1.0km
MP=17, NP=241
scale height (km)
input kernel
0
5
10
15
20
25
30
0.0
0.1
0.2
0.3
0.4
0.5
0.6
0.7
0.8
0.9
1.0
1.1
1.2

Figure 5b

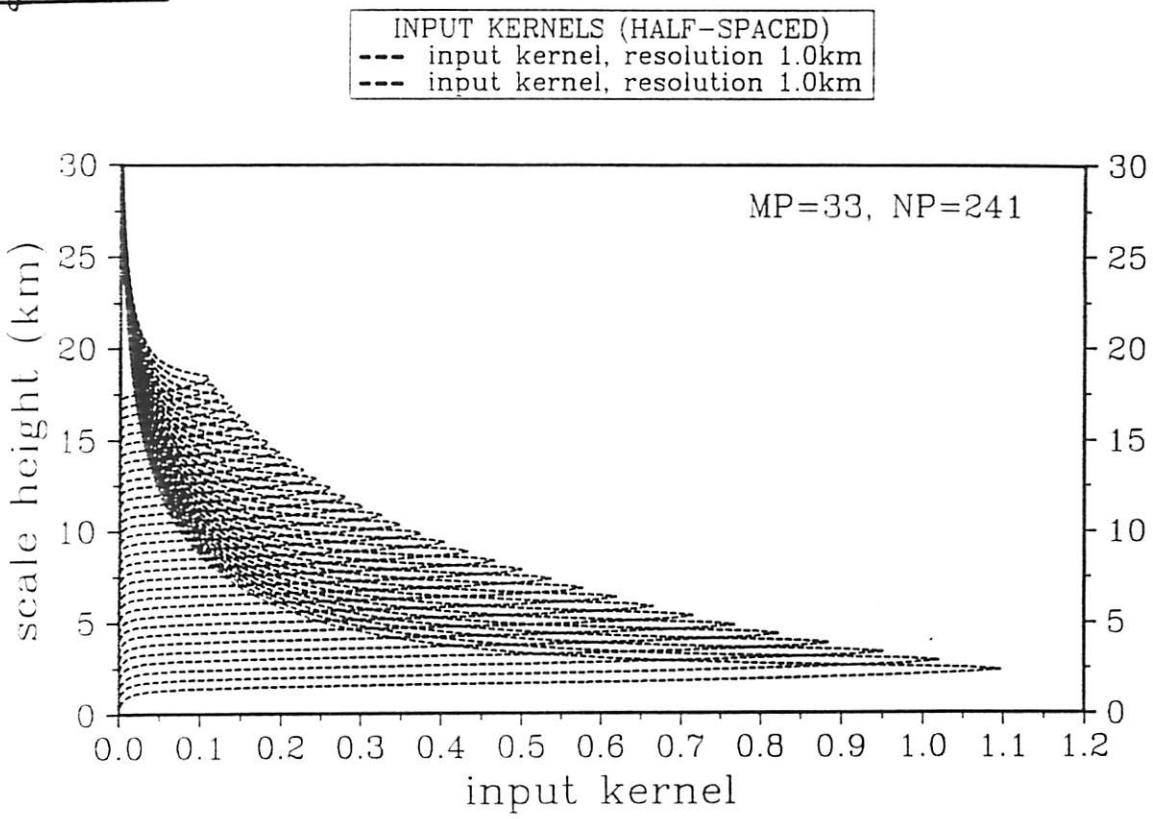

Figure 5c

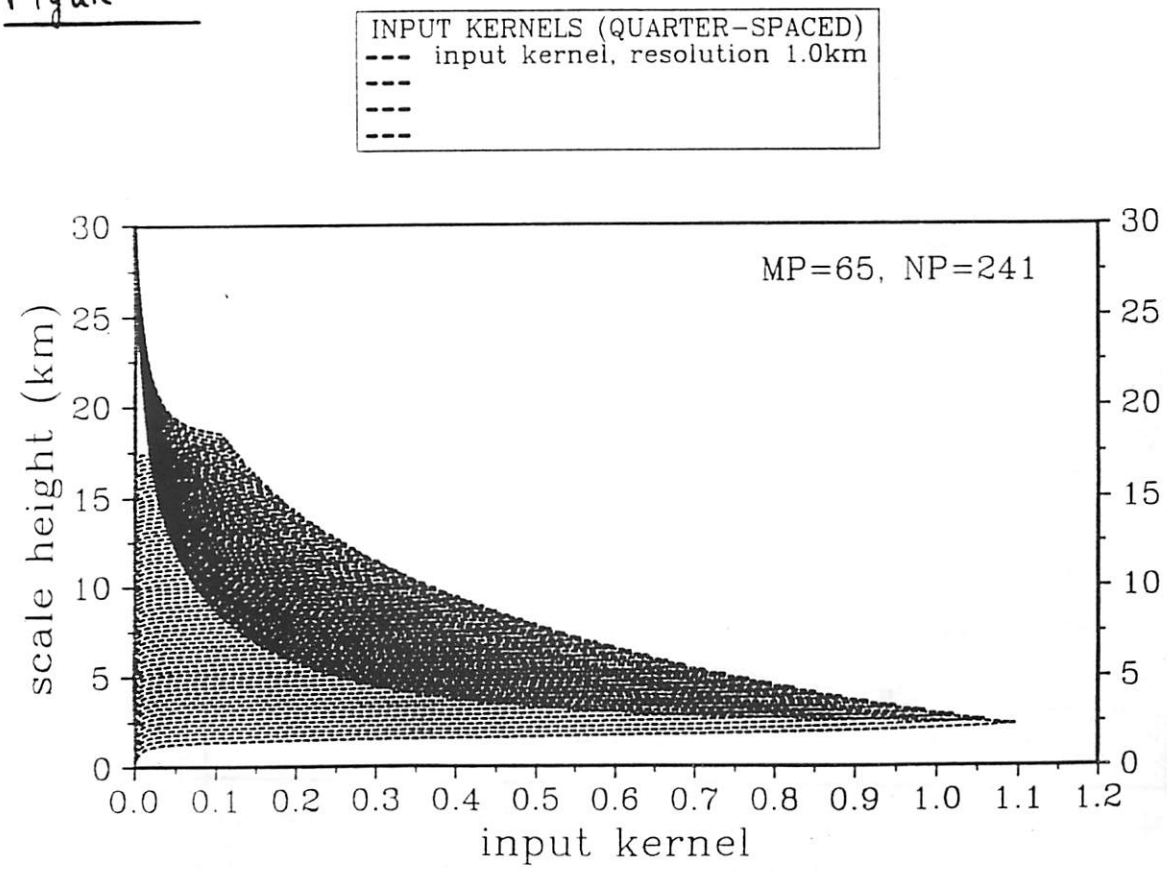

Figure 6a

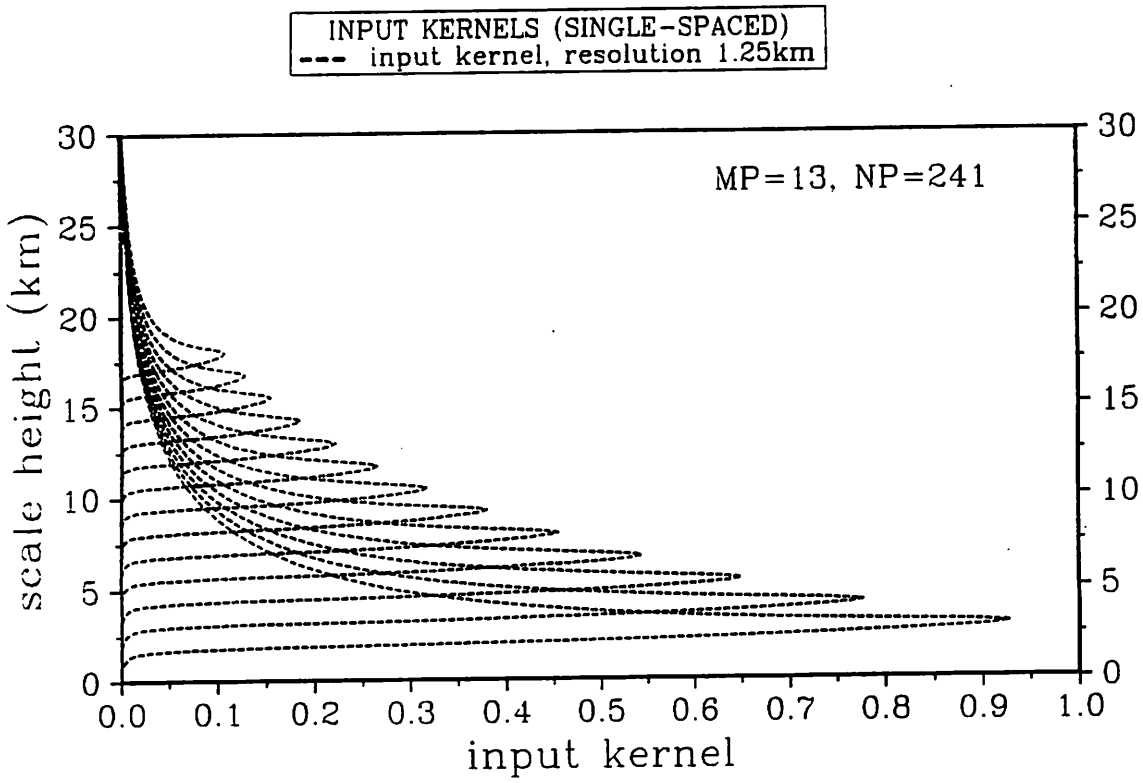

Figure 6b

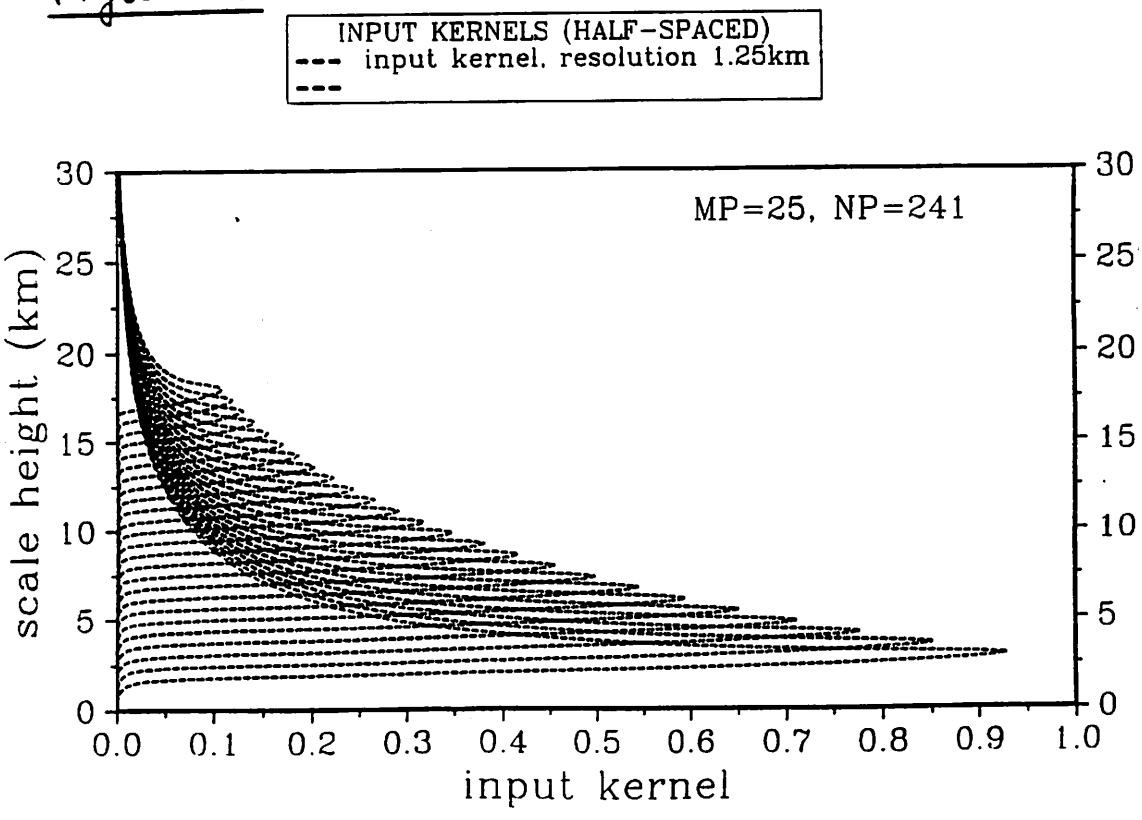

Figure 7a

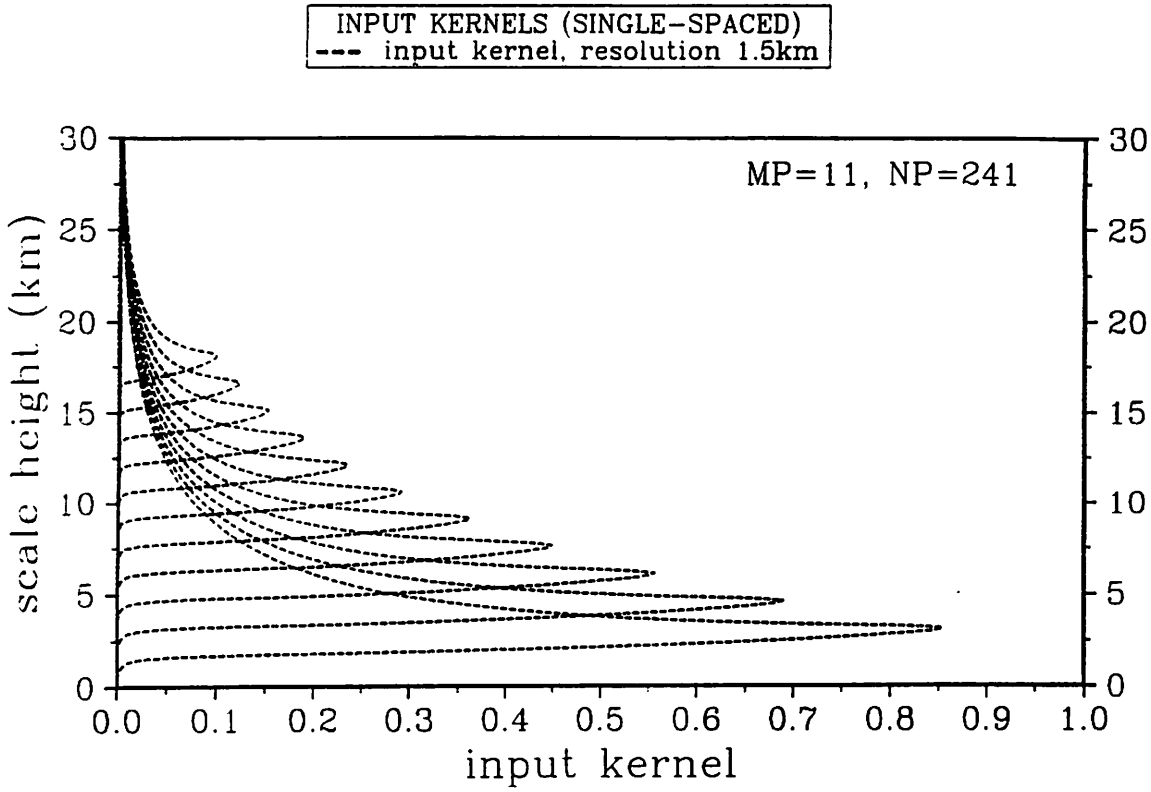

Figure 7b

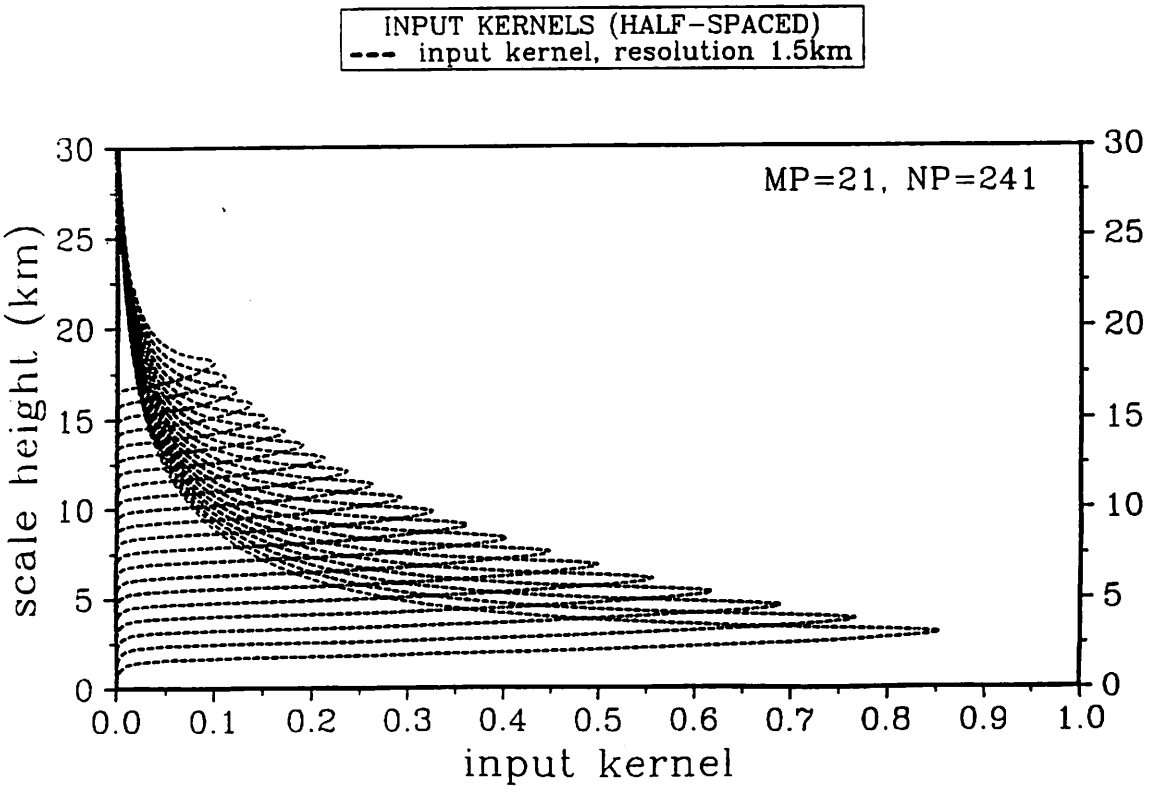

Figure 7c

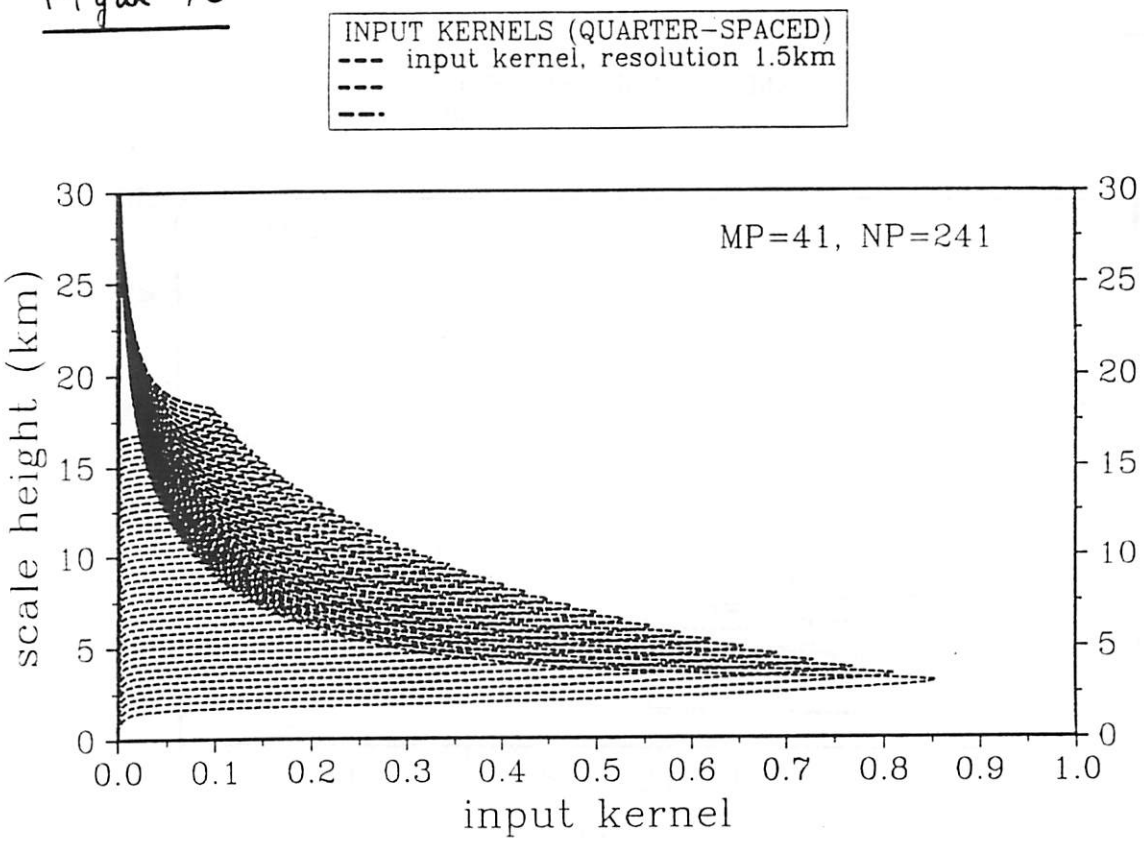
INPUT KERNELS (QUARTER-SPACED)
--- input kernel, resolution 1.5km

--·
MP=41, NP=241
scale height (km)
input kernel
0
5
10
15
20
25
30
0.0
0.1
0.2
0.3
0.4
0.5
0.6
0.7
0.8
0.9
1.0

Figure 8a

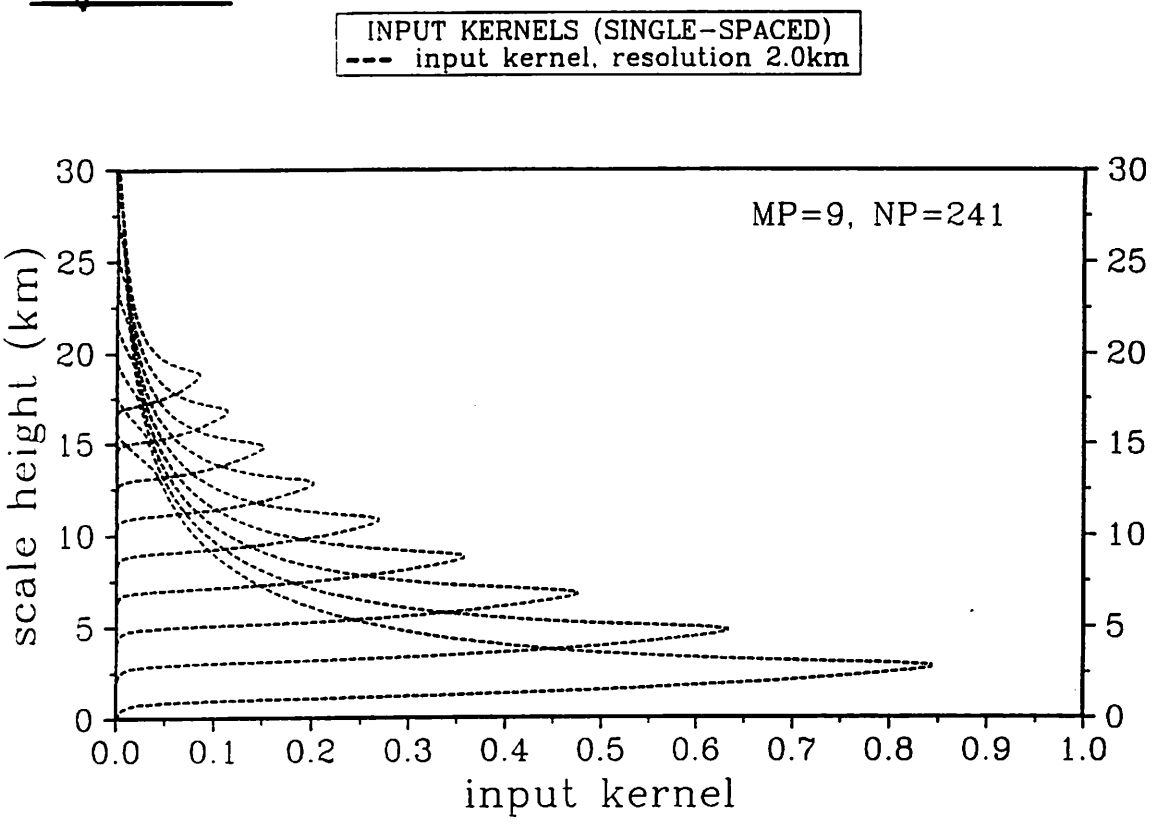

Figure 8b

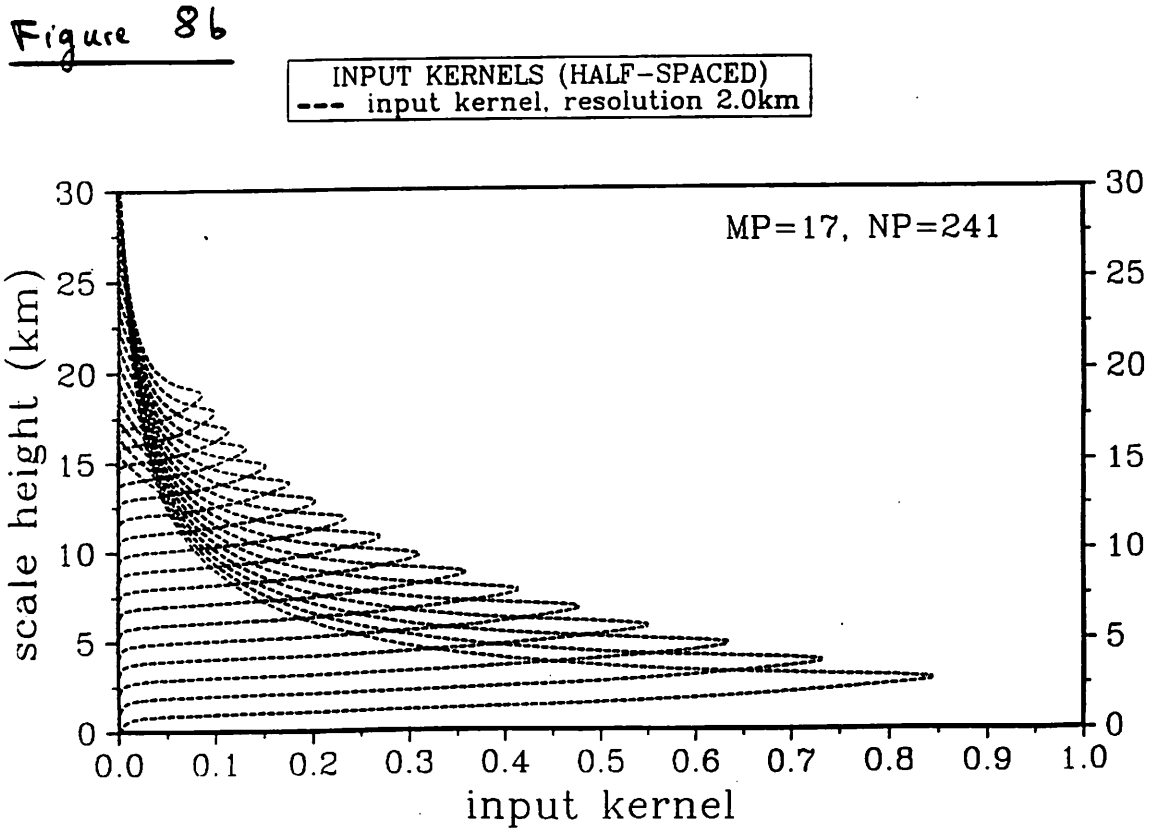

Figure 8c

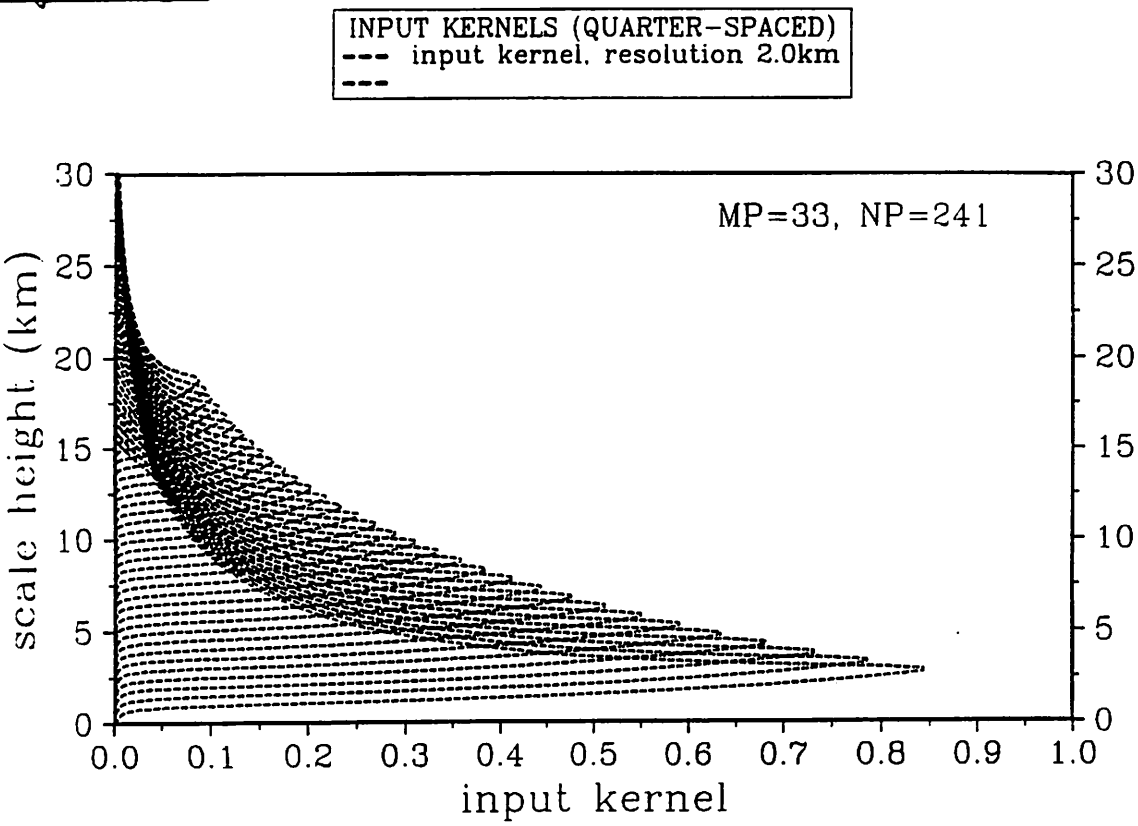
INPUT KERNELS (QUARTER-SPACED)
--- input kernel, resolution 2.0km

MP=33, NP=241
scale height (km)
input kernel
0
5
10
15
20
25
30
0.0
0.1
0.2
0.3
0.4
0.5
0.6
0.7
0.8
0.9
1.0

Figure 9a

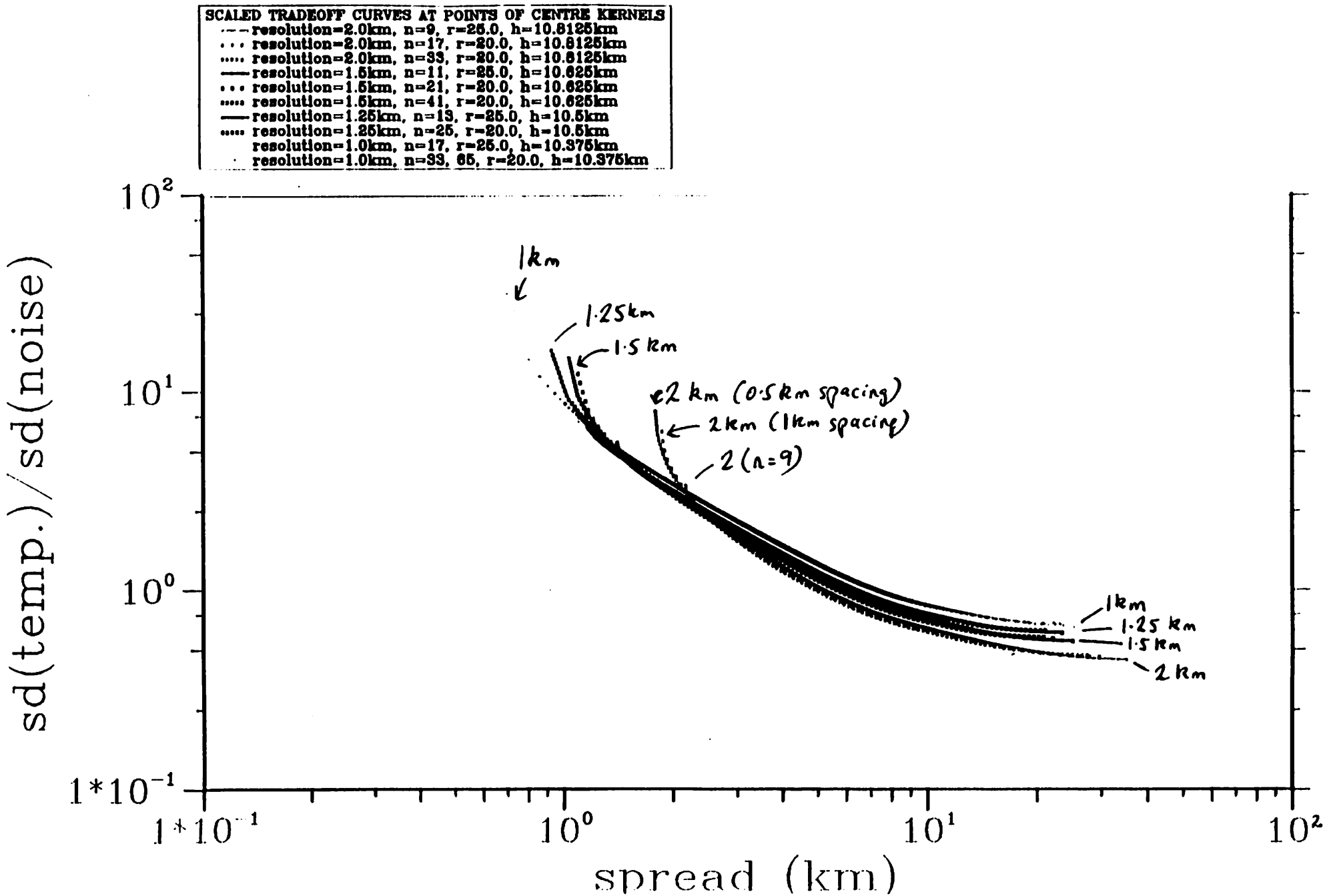
SCALED TRADEOFF CURVES AT POINTS OF CENTRE KERNELS
resolution=2.0km, n=9, r=25.0, h=10.8125km
resolution=2.0km, n=17, r=20.0, h=10.8125km
resolution=2.0km, n=33, r=20.0, h=10.8125km
resolution=1.5km, n=11, r=25.0, h=10.625km
resolution=1.5km, n=21, r=20.0, h=10.625km
resolution=1.5km, n=41, r=20.0, h=10.625km
resolution=1.25km, n=13, r=25.0, h=10.5km
resolution=1.25km, n=25, r=20.0, h=10.5km
resolution=1.0km, n=17, r=25.0, h=10.375km
resolution=1.0km, n=33, 65, r=20.0, h=10.375km
sd(temp.)/sd(noise)
spread (km)
1km
1·25km
1·5km
2 km (0·5km spacing)
2km (1km spacing)
2 (n=9)
1km
1·25 km
1·5km
2 km

Figure 9b

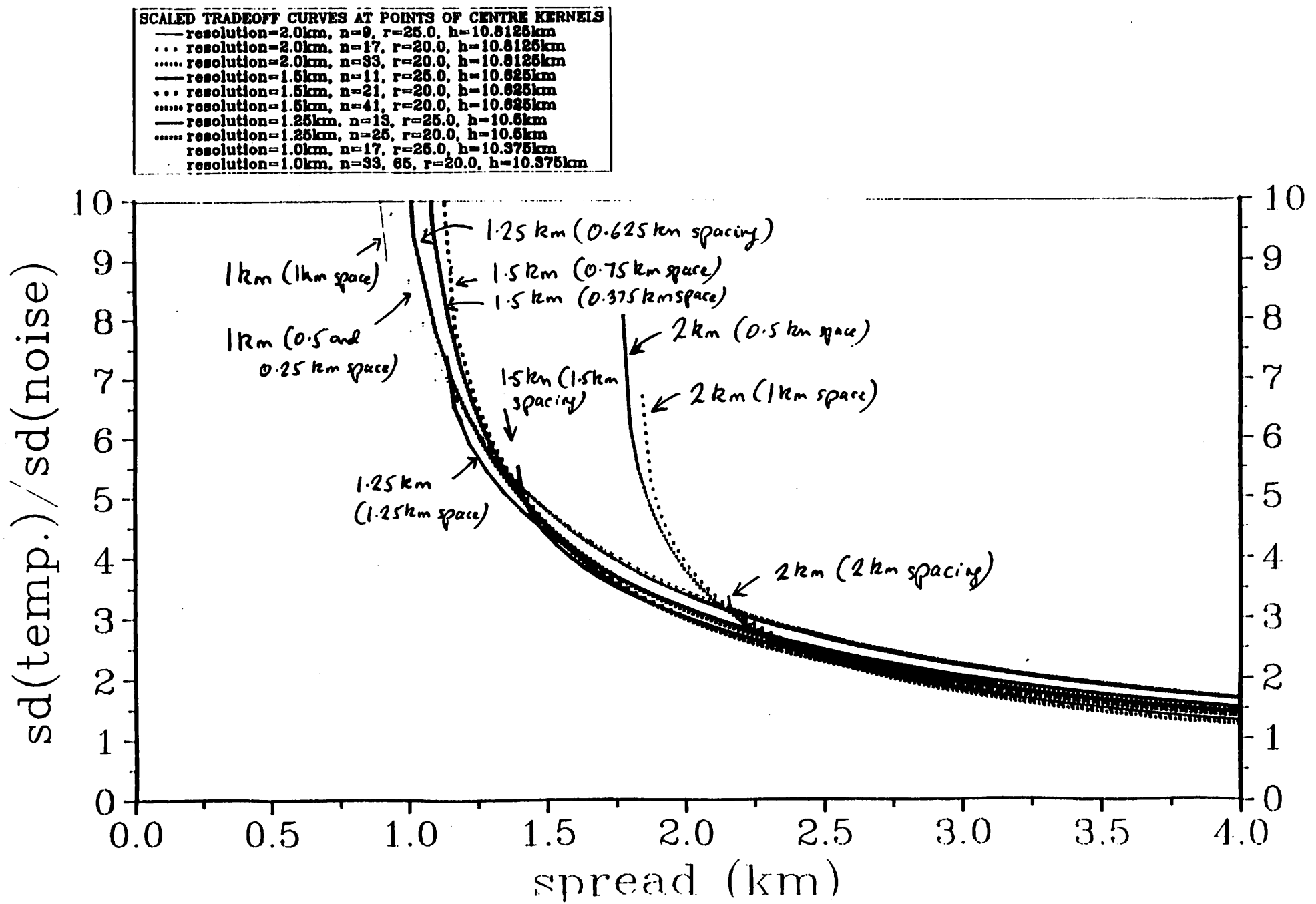
SCALED TRADEOFF CURVES AT POINTS OF CENTRE KERNELS
resolution=2.0km, n=9, r=25.0, h=10.8125km
resolution=2.0km, n=17, r=20.0, h=10.8125km
resolution=2.0km, n=33, r=20.0, h=10.8125km
resolution=1.5km, n=11, r=25.0, h=10.625km
resolution=1.5km, n=21, r=20.0, h=10.625km
resolution=1.5km, n=41, r=20.0, h=10.625km
resolution=1.25km, n=13, r=25.0, h=10.5km
resolution=1.25km, n=25, r=20.0, h=10.5km
resolution=1.0km, n=17, r=25.0, h=10.375km
resolution=1.0km, n=33, 65, r=20.0, h=10.375km
1·25 km (0·625 km spacing)
1·5 km (0·75 km space)
1·5 km (0·375 km space)
2 km (0·5 km space)
2 km (1 km space)
1 km (1 km space)
1 km (0·5 and 0·25 km space)
1·5 km (1·5 km spacing)
1·25 km (1·25 km space)
2 km (2 km spacing)
sd(temp.)/sd(noise)
spread (km)
0.0
0.5
1.0
1.5
2.0
2.5
3.0
3.5
4.0
0
1
2
3
4
5
6
7
8
9
10

Figure 10a

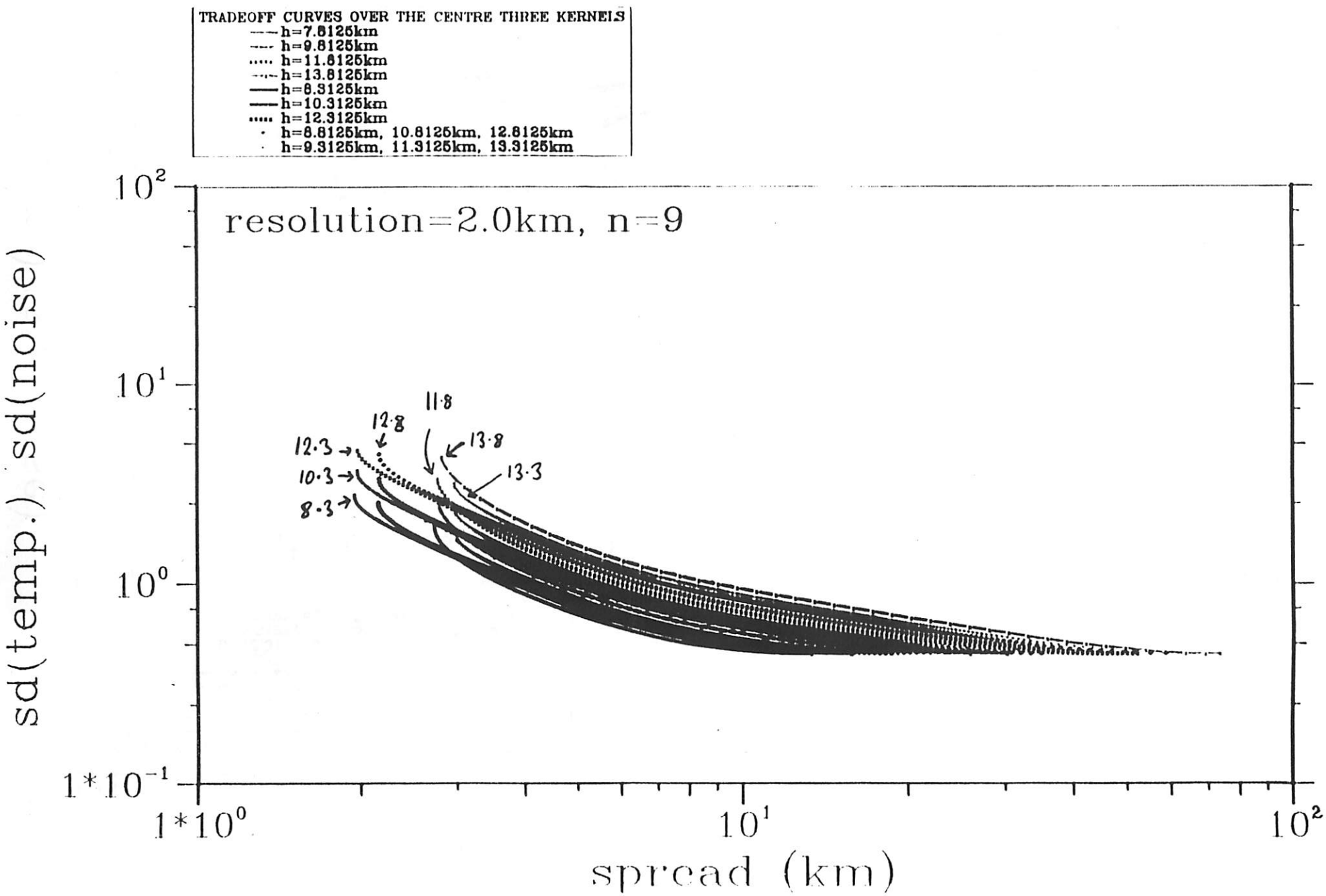
TRADEOFF CURVES OVER THE CENTRE THREE KERNELS
h=7.8125km
h=9.8125km
h=11.8125km
h=13.8125km
h=8.3125km
h=10.3125km
h=12.3125km
h=8.8125km, 10.8125km, 12.8125km
h=9.3125km, 11.3125km, 13.3125km
resolution=2.0km, n=9
sd(temp.), sd(noise)
spread (km)
10^2
10^1
10^0
$1*10^{-1}$
$1*10^0$
10^1
10^2
11·8
12·8
13·8
13·3
12·3
10·3
8·3

Figure 10b

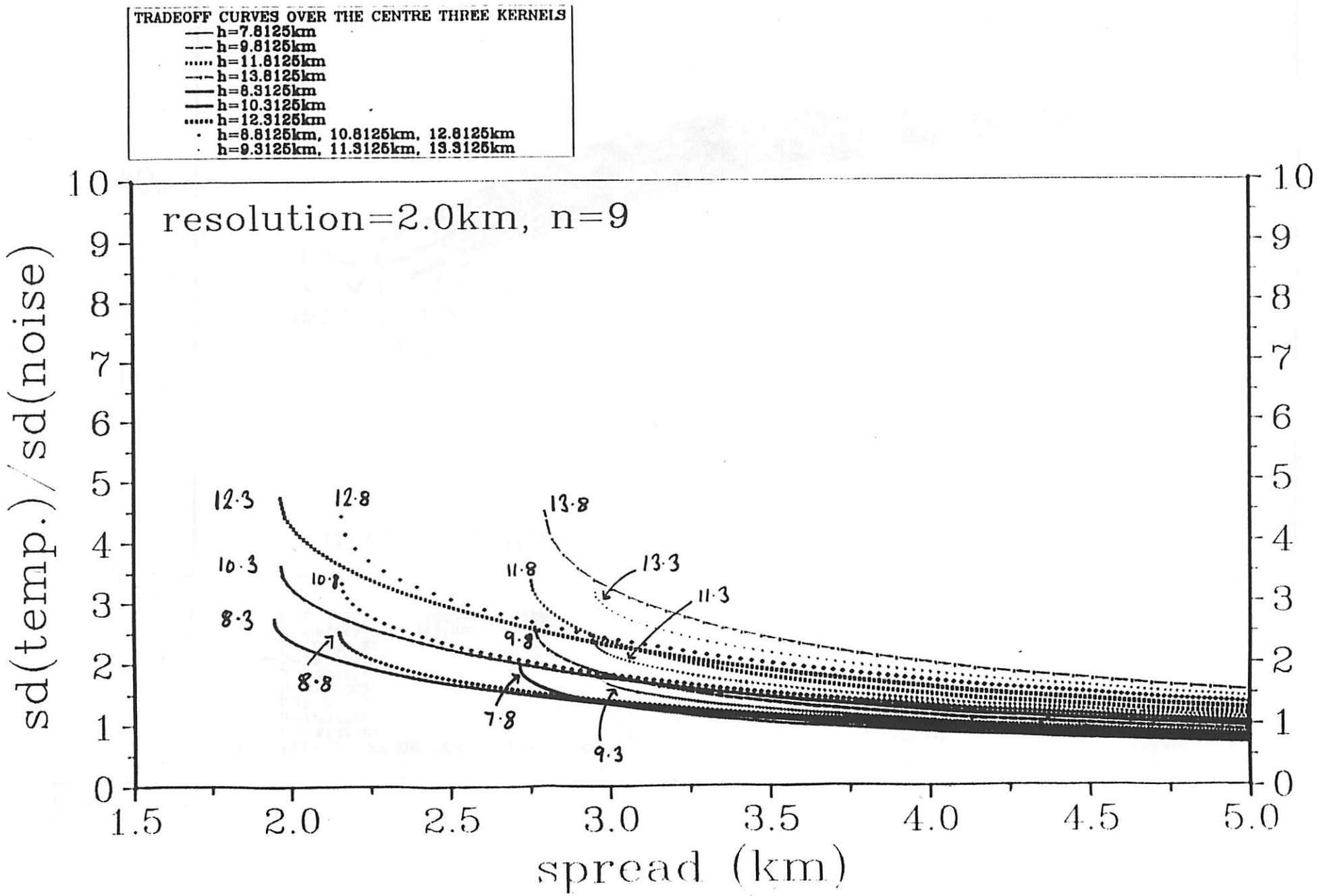
TRADEOFF CURVES OVER THE CENTRE THREE KERNELS
h=7.8125km
h=9.8125km
h=11.8125km
h=13.8125km
h=8.3125km
h=10.3125km
h=12.3125km
h=8.8125km, 10.8125km, 12.8125km
h=9.3125km, 11.3125km, 13.3125km
resolution=2.0km, n=9
sd(temp.)/sd(noise)
spread (km)
12·3
12·8
13·8
10·3
10·8
11·8
13·3
11·3
8·3
9·8
8·8
7·8
9·3
0
1
2
3
4
5
6
7
8
9
10
1.5
2.0
2.5
3.0
3.5
4.0
4.5
5.0

Additional figure

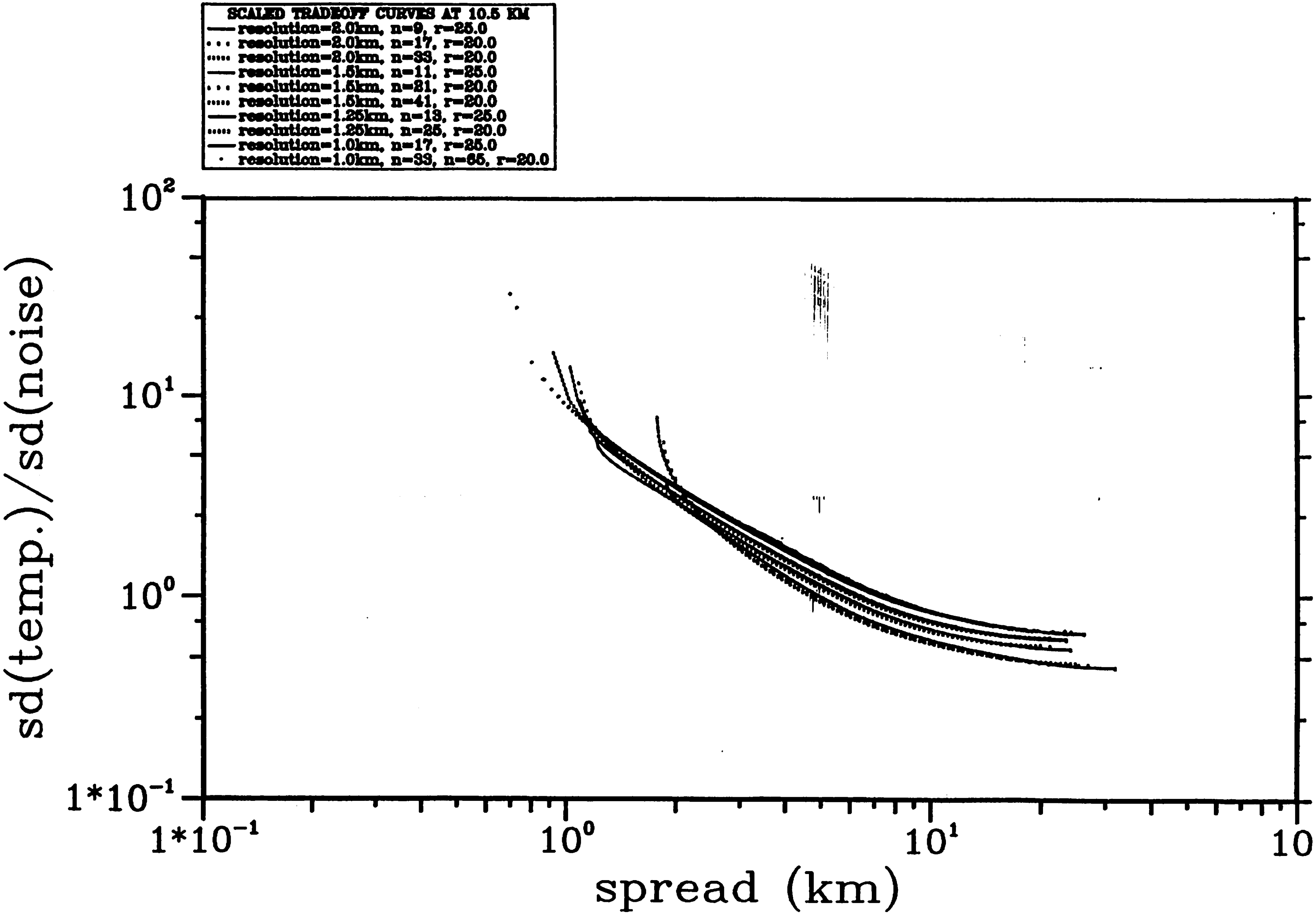

Additional Figure